Water Science & Technology

Water Science & Technology Vol 87 No 8, 1803 doi: 10.2166/wst.2023.102

Catalytic ozonation of *N*-methyldiethanolamine over mixed oxides derived from Mg/Fe-LDH

Nabil Boucenna[a,*], Fatiha Mokhtari-Belkhadem[a], Ali Bouteiba[b], Karima Sahel[a], Francisco Medina[c] and Mourad Lounis[d]

[a] Laboratoire des Éco-Matériaux, Fonctionnels et Nanostructures, Faculté de Chimie, Université des Sciences et de la technologie d'Oran (USTO M. B), BP 1505 El M'naouar, Oran 31000, Algeria
[b] Laboratoire de Chimie des Matériaux Inorganiques et Application (LCMIA), Faculté de Chimie, Université des Sciences et de la technologie d'Oran (USTO M. B), BP 1505 El M'naouar, Oran 31000, Algeria
[c] Departament d'Enginyeria Química, Universitat Rovira i Virgili, Tarragona 43007, Spain
[d] Laboratoire FIMA, Faculté de Science et de la Technologie, Université Djilali Bounaama, Khemis Miliana 44225, Algeria
*Corresponding author. E-mail: nabilboucenna@ymail.com; nabilboucenna@univ-usto.dz

NB, 0000-0003-3521-1679

ABSTRACT

The aim of this study was to evaluate the efficiency of catalytic ozonation to increase the degradation of aqueous *N*-methyldiethanolamine (MDEA) solutions, using two lamellar double hydroxides, namely Mg_xFe-LDH with $x = Mg/Fe = 2, 3$, were synthesized by the simple and rapid co-precipitation method. Then, the obtained materials were calcined at 400 °C for 6 h. The calcined products were respectively designated as $HTcMg_2Fe$ and $HTcMg_3Fe$, and characterized by powder X-ray diffraction (XRD), N_2 physisorption (BET), Fourier transform infrared spectra (FT-IR), and scanning electron microscopy (SEM). The powders produced were used in the ozonation reaction to remove MDEA from aqueous solutions. Experimental results showed that the highest MDEA removal efficiency is in the catalytic ozonation process. Under the optimal conditions for heterogeneous catalytic ozonation of MDEA: initial concentration of 4 Wt% MDEA, 30 °C, catalyst mass of 30 mg/100 ml solution, and contact time of 60 min. The results showed the highest percentage of COD removal, which was up to 80.76% for $HTcMg_2Fe$ higher than that of $HTcMg_3Fe$ 80.36%.

Key words: catalytic ozonation, degradation *N*-methyldiethanolamine, layered double hydroxides, oxidation

HIGHLIGHTS

- Synthesis and characterization of Mg/Fe-LDH and its calcined product.
- Catalytic ozonation of *N*-methyldiethanolamine over mixed oxides derived from Mg/Fe-LDH.
- For the MDEA removal efficiencies, the experimental parameters were optimized.

GRAPHICAL ABSTRACT

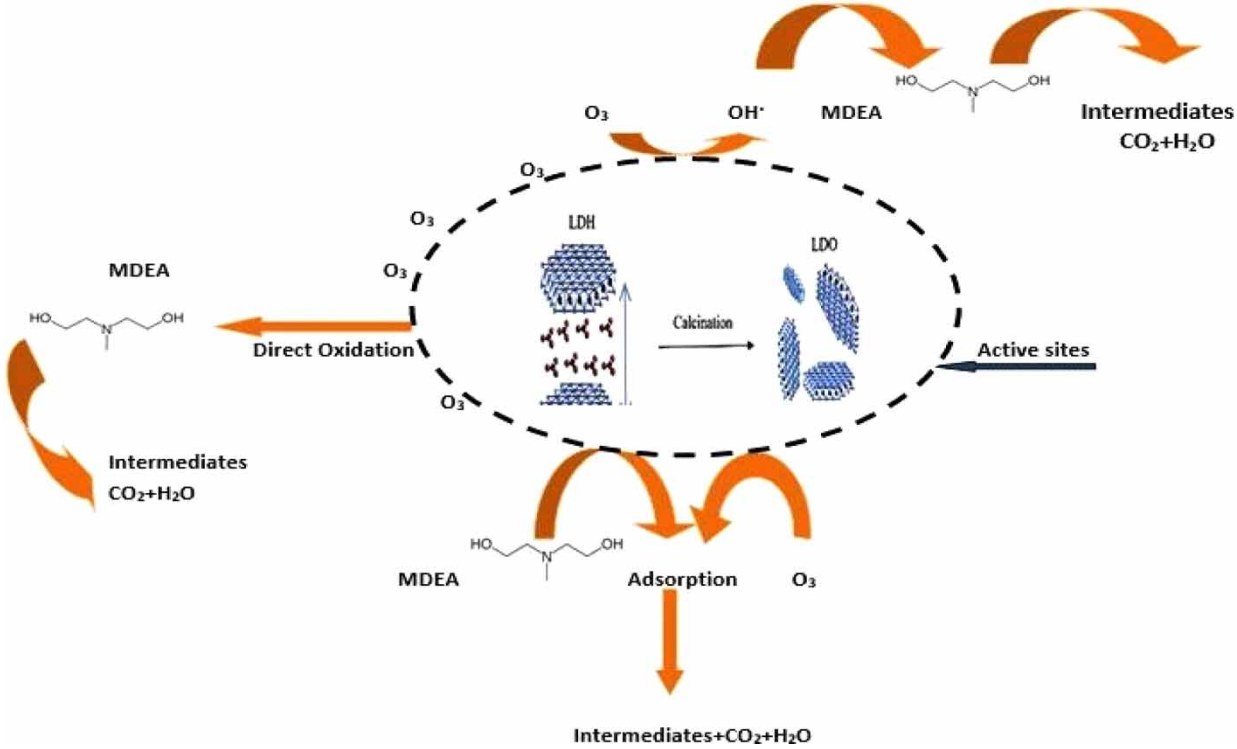

1. INTRODUCTION

The MDEA (*N*-methyldiethanolamine) is widely employed in natural gas processing plants to remove acid gases (CO_2 and H_2S) from raw natural gas (Laila *et al.* 2018). However, a difficulty develops during the regeneration process in the gas purification, when a small amount of non-biodegradable alkanolamine is discharged in the wastewater. The COD of the released wastewater containing amine was high. The purpose of this research was to assess the efficiency of catalytic ozonation reaction, which improves the removal of aqueous methyldiethanolamine and can be used as a pre-treatment before a biological process using the system (catalyst + O_3). Currently, there is a great deal of research on the treatment of alkanolamines contained in wastewater for their toxicity, the use of adsorbents as (activated carbon, chitosan, alumina, zeolite) such as the benefit of using this method to reuse these alkanolamines in the trial (Razali *et al.* 2010). Furthermore, there are many techniques in the field of wastewater treatment for the removal of solids and oil, grease, biodegradable or non-biodegradable organic compounds, and toxic molecules (Haithem *et al.* 2019) Such these techniques applied alone or in cascade improve the level of treatment. Advanced oxidation processes (AOPs) occupy a very important place among the different treatment technologies; have been considered as popular techniques to treat the high concentration of organic contaminants in wastewater. However, we report the treatment methods such as the application of AOP (UV/Fenton, O_3/Ultraviolet, O_3/H_2O_2, UV/H_2O_2, UV/TiO_2) are of the most alternative techniques for the destruction of many other organic matters in wastewater and effluents. Several AOPs have been observed in the literature such as the heterogeneous Fenton degradation of persistent organic pollutants using natural chalcopyrite: effect of water matrix and catalytic mechanism (Jiapeng *et al.* 2022), additionally, these AOPs are very interesting alternatives for the degradation of non-biodegradable organic pollutants by the biological treatment process, such these techniques are based on the generation and use of a powerful oxidant especially the hydroxyl radical ($OH^{\bullet}$) which can be produced by the photochemical and non-photochemical process, while attack the pollutant and form the degraded product (Che *et al.* 2014). In addition, the catalytic ozonation is one of these processes; such that the catalyst provides better performance both in terms of reaction rate and energy consumption (Legube & Karpel 1999). Overall, the efficiency of the oxidation and the fact that it does not form solid residues, such as sewage sludge, are the main advantages of AOP. In the other hand, the major disadvantage generally lies in the high cost of operation due to energy needs. This

hinders industrial development a lot in technology according to a recent study (Oller *et al.* 2011). Currently, ozone with a redox potential of (2.07 V), as a strong oxidant, has drawn increasing attention in various environmental systems for potential oxidant capacity. Ozone reacts rapidly with organic substances in aqueous solution in two ways: direct reaction with molecular O_3 or indirect reaction with the active radicals, such hydroxyl radicals (OH˙) (redox potential of 2.33 V), react with most of the pollutants no selectively, destroying them and converting into harmless organic compound's such as CO_2 and H_2O (Hrvoje *et al.* 2006; Violante *et al.* 2010). O_3 molecules react selectively with the electron-rich compounds, so the reaction rate is quite slow for some other organic compounds such as pesticides and increases energy consumption for ozone production. These are examples of ozone application limitations for the direct removal of pollutants. As a consequence, the application of some combined oxidation technologies, such as catalytic ozonation facilitates the depletion of ozone, and the formation of hydroxyl radicals (OH˙). Recently, the process of catalytic ozonation has received more attention due to its effectiveness in treating wastewater (Lim *et al.* 2020). Moreover, the reaction can be run at ambient conditions of temperature and pressure with complete mineralization of the organic matter into carbon dioxide and water.

In this context, several materials have been used as catalysts in the catalytic ozonation, such as metal oxides (MnO_2, FeOOH, Fe_2O_3, MgO, TiO_2, etc.) (Bing *et al.* 2019a, 2019b), support metals (Cu, Ru, Pt, Co), zeolites modified with metals, activated carbon, and mesoporous structures (Hui *et al.* 2020). The mixed metal oxides have also been used in these reactions, which are promising catalysts because of their higher reactivity (Mahesh *et al.* 2014). Hence, various research papers dealing with LDH materials have been published (Nazrizawati *et al.* 2022). However, the synthesis of highly dispersed mixed oxides can be obtained from lamellar double hydroxides (LDHs) structures by calcination of parent LDH (Mir Saeed *et al.* 2021). These structures are considered to be a class of anionic clays and have received much attention in the field of catalysis because of their interesting physicochemical properties (Vaccari 1999). Moreover, they are used in hydrogen generation reactions (Bert *et al.* 2001), 5-hydroxymethyl furfural formation (Xiangbo *et al.* 2021), photocatalysis (Haithem *et al.* 2019), oxidative dehydrogenation of ethanol to acetaldehyde (Haolan *et al.* 2022), and as a potential adsorbent on the removal of pollutants from the environment due to their high surface area, high anion exchange capacity, and good thermal stability (Amy-Louise *et al.* 2021). Suggesting, the degradation in tetracycline for copper-based catalysts from electroplating sludge by ultrasound treatment and their antibiotic degradation was performed and the results showed that the product had very good performance over a wide pH range (2–11). At an initial pH = 2, the copper-based catalysts could degrade 91.9% of 50 mg/L tetracycline aqueous solution within 30 min (Zhenxing *et al.* 2023). So far, various catalysts have been investigated for AOP such as LDHs (layered double hydroxides), Haung *et al.* (2020) elaborated the Ni_2Fe-LDHs and used them as a catalyst in the heterogeneous catalytic ozonation of Bisphenol A, they found that a Ni:Fe ratio of 3:1 was an excellent catalyst for complete removal of Bisphenol A (Yuanxing *et al.* 2019). Hence, the degradation of aniline by the ozonation process using Co_2Fe-LDH and Co_2Al-LDH layered double oxides was studied (Yuanfeng *et al.* 2020). Furthermore, they used the Mg_2Al-LDH as a catalyst for the decomposition of *p*-nitroaniline from aqueous solutions by ozonation (Mohammad *et al.* 2020). Recently, several synthesis methods can be used to prepare LDH, among them; the co-precipitation reaction under mild conditions is relatively a simple and economical method (Ali *et al.* 2020a, 2020b). The LDH structure is defined as $[M^{2+}_{(1-x)}\ M^{3+}_{x}\ (OH)_2]^{x+}(A^{n-})\ x/n{\cdot}mH_2O$, where ($\mathbf{M^{2+}} = Mg^{2+}, Ni^{2+}, Co^{2+}, Cu^{2+}, Zn^{2+}$) and ($\mathbf{M^{3+}} = Al^{3+}, Fe^{3+}, Cr^{3+}$) metal cations, $\mathbf{A^{n-}}$ is interlayer exchangeable anions such as NO_3^{2-}, CO_3^{2-}, Cl^-, and I^- and $\boldsymbol{m}$ is the number of water molecules (Ali *et al.* 2020a, 2020b).

In this research, two mixed oxide solids were prepared by the calcination of Mg_2Fe-LDH and Mg_3Fe-LDH. The powders obtained were denoted as $HTcMg_2Fe$ and $HTcMg_3Fe$, respectively, were used in the catalytic ozonation reaction of *N*-methyldiethanolamine to reduce it in wastewater due to its toxicity and negative environmental impact. The structural formula of MDEA is shown in Figure 1. Subsequently, the prepared materials were characterized by various physicochemical techniques (X-ray diffraction (XRD) (Shanza *et al.* 2020), Fourier transform infrared (FT-IR), differential thermal and thermogravimetric analysis (DTA and TGA), N_2 adsorption–desorption isotherms (BET), and scanning electron microscopy (SEM).

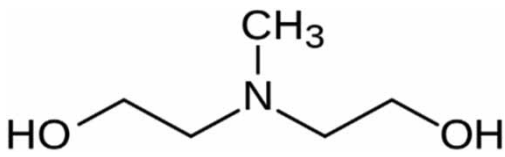

Figure 1 | The structure of MDEA.

2. EXPERIMENTAL

2.1. Materials

The chemical reagents used were: sodium hydroxide pellets (Fisher Scientifique, 99%), hydrochloric acid (Fisher Scientifique, 36%), iron (III) chloride hexahydrate $FeCl_3{\cdot}6H_2O$ (Prolabo, 99.8%), magnesium chloride hexahydrate $MgCl_2{\cdot}6H_2O$ (prolabo, 99.9%), and deionized water purified by the Water Purification System Milli-Q (MERCK).

2.2. Synthesis procedure

For the synthesis of LDHs phases, we follow the experimental protocol based on the co-precipitation method (Aaron & Dahn 2019; Ali *et al.* 2020a, 2020b). In a typical synthesis, magnesium chloride $MgCl_2{\cdot}6H_2O$ (0.2 mol for ratio 2 and 0.3 mol for ratio 3) and iron chloride $FeCl_3{\cdot}6H_2O$ (0.1 mol) were continuously stirred into NaOH solutions at pH 10 and room temperature of 25 °C. The solution while stirring at 700 rpm for 24 h. The synthesis was carried out under an inert atmosphere (N_2 gas bubbling). Then, the suspensions obtained were hydrothermally treated at a temperature of 80 °C for 24 h. To collect the products, the suspensions were centrifuged and rinsed five times with deionized water. Ultimately, the products were obtained by drying the powders in an oven at a temperature of 65 °C for 24 h to achieve the Mg_2Fe-LDH and Mg_3Fe-LDH. Activation of the powders was conducted via calcination in a muffle furnace at 400 °C in an air atmosphere for 6 h. The Mg_2Fe-LDH after calcination gives a product denoted as $HTcMg_2Fe$ and the second Mg_3Fe-LDH gives a product designated as $HTcMg_3Fe$.

2.3. Characterization methods

XRD patterns were recorded of $2\ominus = (5–70°)$ using a Bruker-AXS Advance diffractometer (40 kV, 30 mA, radiation $\lambda =$ 0.15406 nm). FT-IR using a tensor 27 spectrometer (Bruker Optik GmbH, Germany). TG was recorded by thermal analysis using the TA Micrometrics 2050 TGA in the range of 30–800 °C with a heating rate of 5 °C/min. The surface areas were determined at 77.35 K by application of the N_2 adsorption–desorption isotherms (BET) method in a Micromeritics Tristar 3000 after degassing the sample *in vacuo* under nitrogen flow overnight at 150 °C L (Laila *et al.* 2018). The pH value and electrical conductivity were measured by a pH meter inolab pH 730 (WTW) and an electrical conductivity meter inolab cond 730 (WTW), respectively.

2.4. Catalytic ozonation process of MDEA

We were interested in this study to determine the removal efficiency of an MDEA contained in a synthetic aqueous solution by adsorption, catalytic, and non-catalytic ozonation. We have suggested different parameters such as contact time, catalyst dose, pH contact solution, and MDEA concentration were optimized to achieve maximum removal of MDEA by several processes. Therefore, a 500 ml capacity quartz tube reactor was used for the adsorption, catalytic ozonation, and ozonation alone. The schematic setup of the experiments is shown in Figure 2. Overall, the ozone gas coming from the ozone generator was introduced through a porous diffuser at the bottom of the reactor under continuous stirring; the residual ozone was captured in a potassium iodide solution (KI). Hence, to determine the adsorption phenomena affect, all solutions while stirring magnetic at 700 rpm without O_3 for 30 min to ensure the establishment of adsorption/desorption equilibrium between the catalysts and MDEA. Then, the solution was exposed to an ozone flow rate 5 mg/min, after that the sample was pipette via the sampling port of the reactor, and then separated from the suspended catalyst particles by filtration through millipore filters (porosity 0.22 μm). Furthermore, the sample was analyzed. In this work, various parameters are studied such as concentrations of MDEA (4, 8, 12, 16, and 20 Wt%), pH (from 3 to 11), the dosage of the catalyst and the time effect.

The chemical oxygen demand (COD) analysis using the HACH model DR/2800 spectrophotometer (HACH Company, USA) equipped with the HACH test tube.

The COD values were calculated as (Bing *et al.* 2019a, 2019b):

$$\text{COD Removal (\%)} = \frac{(\text{COD}_0 - \text{COD}_t)}{\text{COD}_0} \times 100 \quad (1)$$

where COD_0 and COD_t are initial and appropriate COD readings for MDEA at any time. The amine concentration (Wt%) was measured by using the method procedure (recommended by BASF) with a taschiro indicator, where this method was designated for LNG3 (Algeria Sonatrach Company, Algeria). The hydrochloric acid 0.01N was added to MDEA sample until the solution changed color (Razali *et al.* 2010).

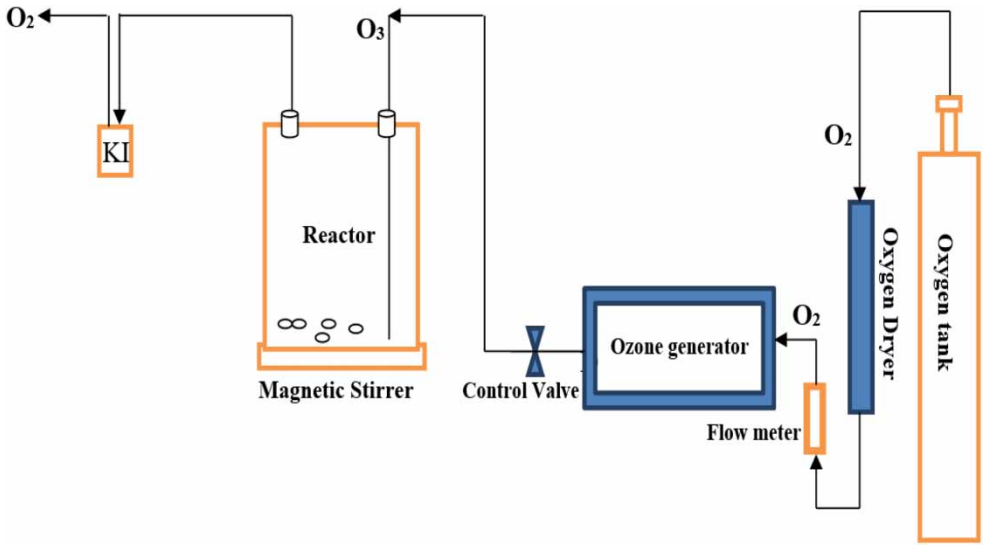

Figure 2 | Schematic diagram of the catalytic ozonation process.

The MDEA content was also analyzed using an automatic titrator (T50 METTLER TOLIDO serial number SNR: B134208930 with a reference electrode DX 200, DGI 111-SG (0–14) pH, (0–80 °C), KCl 3 mol/L AgCL sat).

The weight percentage of MDEA is given by the following method:

$$\text{MDEA (Wt\%)} = \frac{(C_1 V_1) \times 9.25}{W} \tag{2}$$

where C_1 and V_1 are the concentration and the volume of the HCl solution, respectively; W is the weight of MDEA taken. The factor = 9.25 (recommended by BASF).

The remaining of MDEA concentration was calculated as:

$$\text{MDEA Removal (\%)} = \frac{(C_0 - C_t)}{C_0} \times 100 \tag{3}$$

where C_0 is the initial concentration of the sample and C_t is the concentration of the sample at time t.

3. RESULTS AND DISCUSSION

3.1. Structural and chemical characterization

The XRD patterns of the materials are shown in Figure 3(a) and 3(b). As can be seen from Figure 3(a), all the diffraction peaks (003), (006), (012), (015), (018), (110), and (113) are indexed to typical LDHs with rhombohedral symmetry in the space group $R3m$ (JCPDS PDF-96-210-2794) (Masoud *et al.* 2021).

As shown in Figure 3(a), three basal reflections typical of an LDH structure were observed: at 2θ of about 10° for (003), 23° for (006), and 35° for (009) (Ligita *et al.* 2020). Furthermore, the calculated d-spacing and the cell parameters (a and c) are given in Table 1. From this table, the calculated values of parameter a (lattice parameter) with the molar ratio for Mg/Fe = 2 are a little small compared with the lattice parameter for Mg/Fe = 3M. However, a small increase for lattice parameter a with increasing for the molar ratio R = 3 Mg/Fe. Overall, the calcined LDH ($HTcMg_2Fe$ and $HTcMg_3Fe$) are shown in Figure 3(b). It can be seen that the lamellar structure collapsed completely toward the formation of mixed oxides during the calcination process (Esthela *et al.* 2019). The peaks at 2θ = 43.05° and 62.55° which corresponds to MgO (LCPDS 78-0430) (Dhal *et al.* 2015), and at 2θ = 30.1°, 35.5°, 43.06°, 57.0°, and 62.55°, that of the spinel structure of $MgFe_2O_4$ (magnesioferrite) (JCPDS 17-0465) (Yi *et al.* 2021; Lingyu *et al.* 2022).

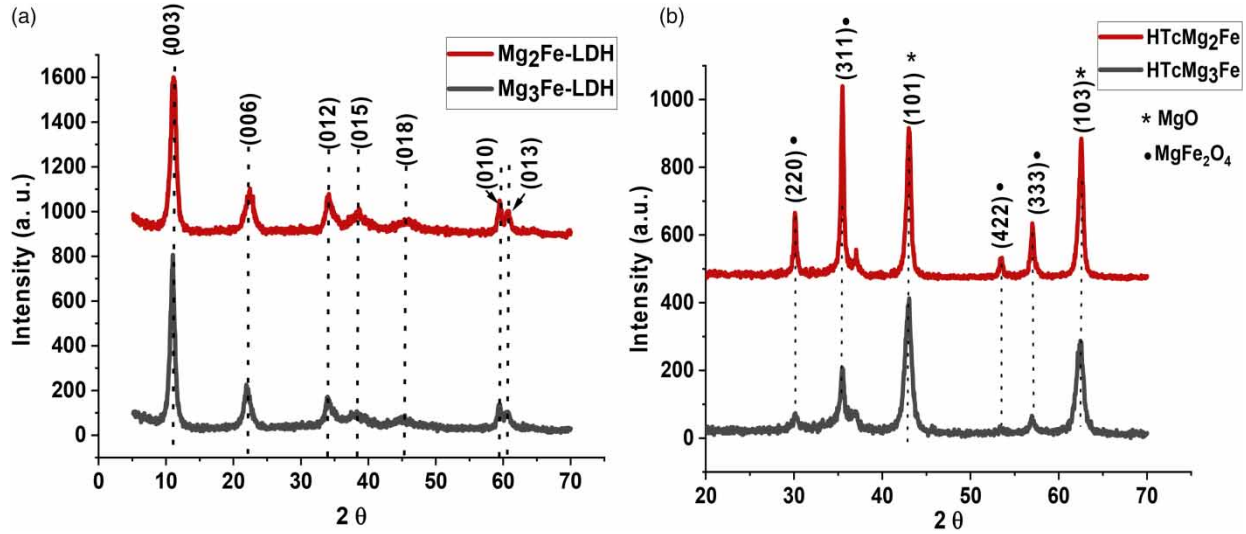

Figure 3 | X-ray diffraction patterns of (a) Mg_2Fe-LDH, Mg_3Fe-LDH and (b) $HTcMg_2Fe$, $HTcMg_3Fe$.

Table 1 | Structural parameters derived from XRD analysis

LDH	d_{003} (Å)	a (Å)	c (Å)	d_{001} (Å)
Mg_2Fe-LDH	7.75	3.01	23.25	1.51
Mg_3Fe-LDH	8.03	3.1	24.09	1.55

Hence, the FT-IR spectra of synthesized materials LDH and HTc are shown in Figure 4(a) and 4(b). The broadband observed at 3,386 cm^{-1} corresponds to the hydrogen bond vibration of OH^-OH_2 and H_2O types of the hydroxyl and water molecules remaining in LDH (Ali *et al.* 2020a, 2020b). The weak band at 1,643 cm^{-1} is assigned to the H–OH bending vibration of interlayer water H_2O molecules. The strong band at 1,360 cm^{-1} is attributed to the ν_3 mode of the interlayer

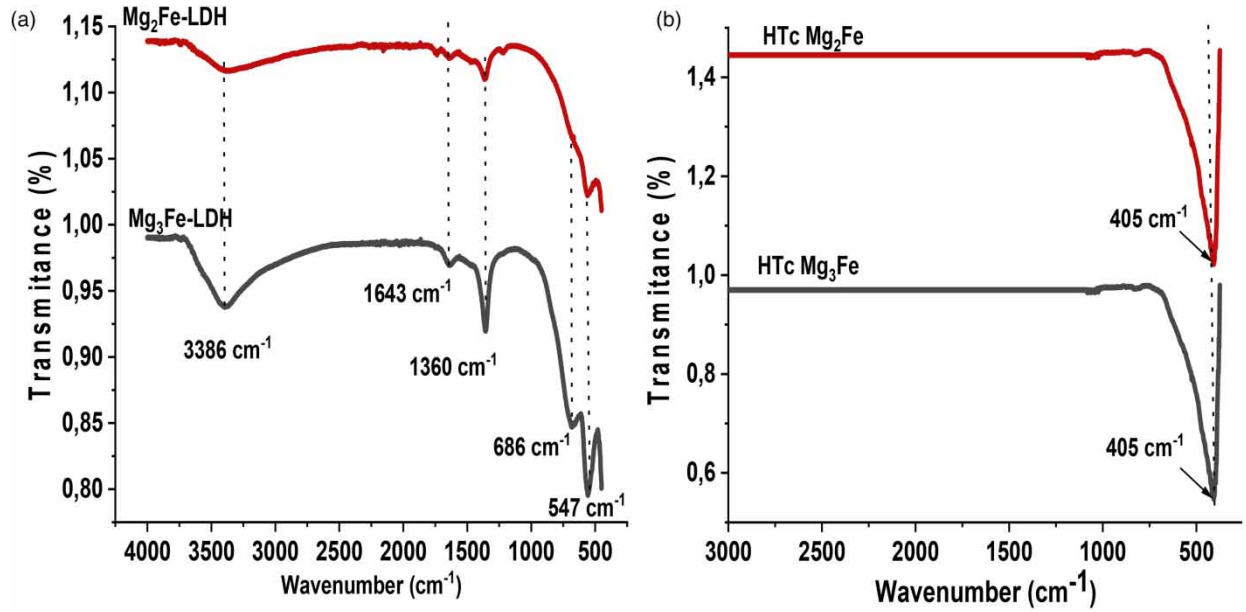

Figure 4 | Fourier transform infrared spectra of (a) LDHs and (b) HTc.

carbonate anions (CO_3^{2-}) remaining in the structure. The bands in the range of 686–547 cm^{-1} are attributed to the metal–oxygen–metal stretch; specifically, the vibrational frequency of 547 cm^{-1} is attributed to the Fe–OH bond, and the band 686 cm^{-1} corresponds to the vibration of O–Fe–O (Fei-Peng *et al.* 2014; Anamália *et al.* 2021).

In addition, the ferrite spinel with the $MgFe_2O_4$ structure has two types of hydroxyl groups on the surface Fe–OH bond attributed 547 cm^{-1}, which are the main active centers for binding various cationic and anionic compounds. In aqueous solutions, an outer layer of hydroxyl groups (surface) is formed on the surface of ferrite spinel (Ligita *et al.* 2020). The surface charge of a metal ferrite depends on the solution pH and can be described using the zero charge point (pH_{pzc}). In the case of $pH < pH_{pzc}$, the surface is dominated by an excess positive charge ($-OH^{2+}$) due to an increase in the number of H^+ ions, as a result, the adsorbent behaves like a Brensted acid. At $pH > pH_{pzc}$, the surface of the adsorbent acquires a negative charge as a result of the deprotonation of hydroxyl groups, and the adsorbent will behave as a Brensted base. Thus, denoting that anions are commonly adsorbed at $pH < pH_{pzc}$ and cations at $pH > pH_{pzc}$ (Ligita *et al.* 2020).

In the case of HTc, the FT-IR spectrum shows complete disappearance of the characteristic bands of water molecules (at about 3,386 cm^{-1}) and the carbonate group CO_3^{2-} (at around 1,360 cm^{-1}). Meanwhile, an increase in the intensity of the bands corresponds to the characteristic vibrations of the M–O bonds (M = Fe or Mg) in the range of 405 cm^{-1} (Shutang *et al.* 2021).

Furthermore, the thermal behavior of both LDHs is shown in Figure 5(a) and 5(b). It can be seen that the peaks at 129 and 124 °C correspond to the loss of physisorbed and interlayer water. The temperatures of 329 and 317 °C correspond to the mass loss due to dehydroxylation, which induces the collapse of the structure through endothermic reactions (Qining *et al.* 2022). In the case of Mg_2Fe-LDH, evolution to cubic periclase (MgO) and amorphous spinel ($MgFe_2O_4$) occurs at 329 °C. The same thermal decomposition profile is observed for Mg_3Fe-LDH.

Figure 6 shows the N_2 adsorption–desorption isotherms of the calcined materials, and the structural parameters of both materials are listed in Table 2. According to the IUPAC classification, both materials are characterized by the same type IV isotherm with an H3-type hysteresis loop, indicating the presence of mesopores in the form of slits (Shutang *et al.* 2021). Figure 6(b) shows the pore size distribution of both. From the BET analysis, the total surface area for $HTcMg_3Fe$ (65.347 m^2/g) is higher than $HTcMg_2Fe$ (32.245 m^2/g) and could help to enhance the catalytic activities.

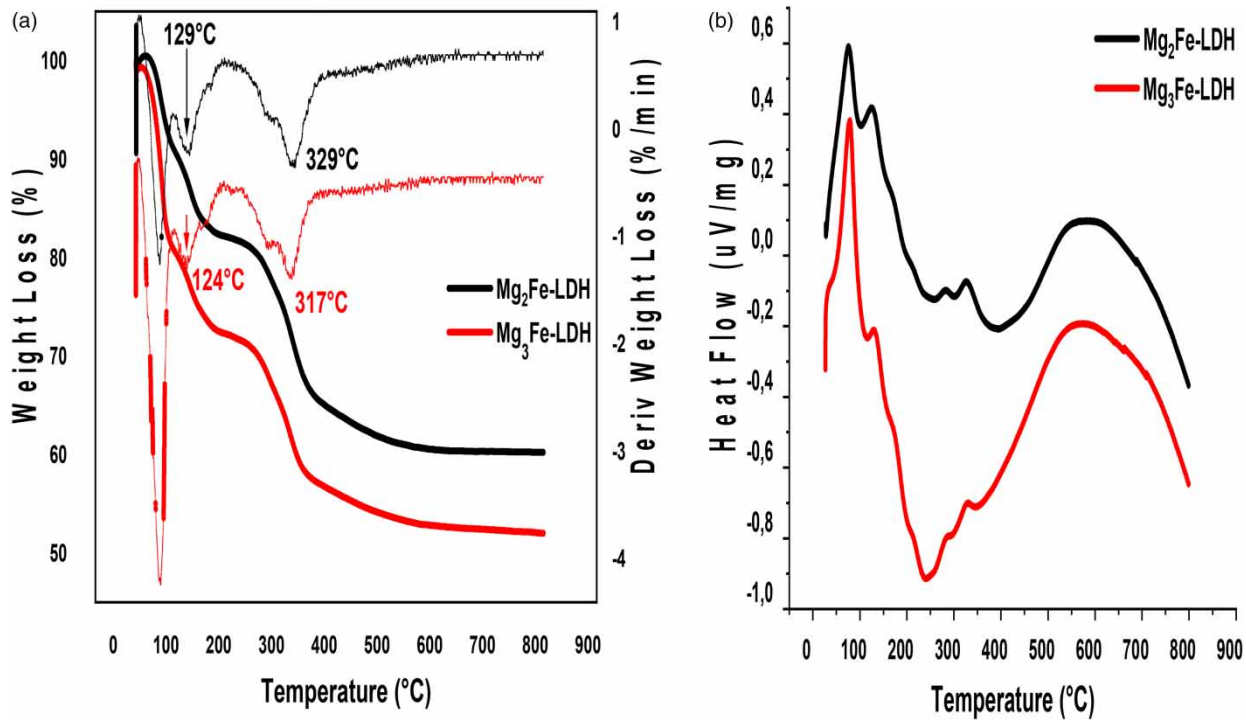

Figure 5 | Thermal analysis of LDHs (a) differential thermal analysis (DTA) and (b) thermogravimetric analysis (TGA).

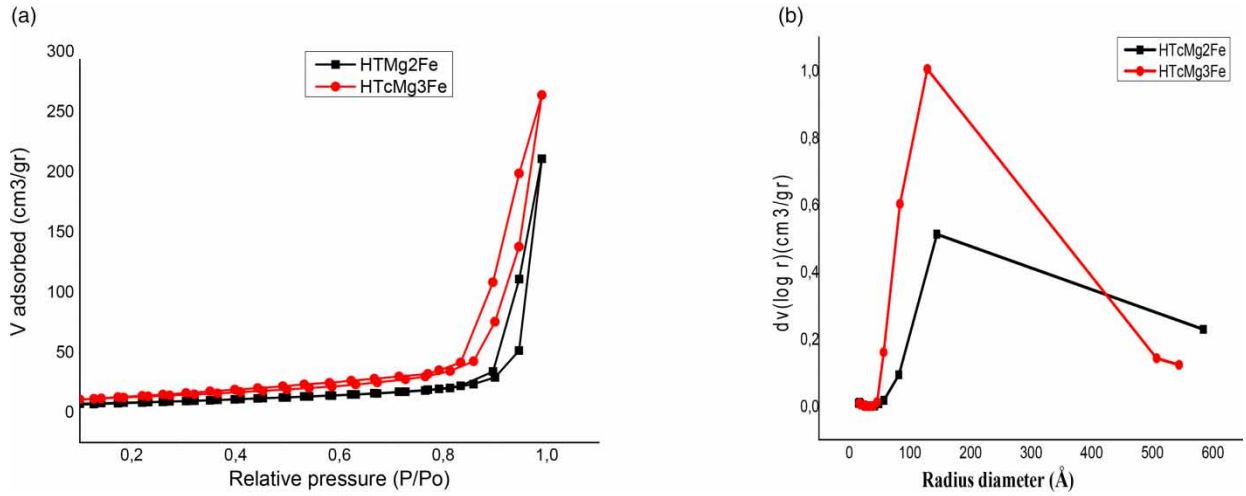

Figure 6 | (a) Isotherms using N_2 adsorption–desorption and (b) pore size distribution curves of $HtcMg_2Fe$, $HTcMg_3Fe$ materials.

Table 2 | Textural properties of activated layered double hydroxides

Catalyst	BET area (m^2/g)	Pore diameter (nm)	Pore volume (cm^3/g)
$HTcMg_2Fe$	32.245	144.645	0.327
$HTcMg_3Fe$	65.347	128.972	0.417

The microstructural and morphological features of the LDH and HTc samples are further explored using (SEM) analysis and their corresponding descriptions are shown in Figure 7(a)–7(d). LDHs particles are irregular plate-like particles characteristic of a stacked sheet structure. The highest aggregation of the particles was found in the case of the HTc materials (Figure 7(b) and 7(c)), indicating that there is the destruction of the lamellar structure during the calcination process.

3.2. Effect of operating parameters on the degradation performance of MDEA

3.2.1. Effect of catalyst mass

The dosage of adsorbent mass is one of the most important influencing parameters in the mass transfer process during the adsorption reaction. This provides the number of active sites capable of interacting with the molecule in solution, which we initially studied the effect of catalyst mass. The adsorption performance of activated materials HTc was investigated for the removal of MDEA-wastewater conditions: (100 ml of a solution containing MDEA (4 Wt%), catalysts dose (10–60 mg), time of 30 min, and pH 10). A 5 ml of each solution was taken and filtered before analysis.

The results illustrated in Figure 8(a) are clearly showed that increasing mass catalysts from 10 to 30 mg increased the percentage of adsorption MDEA from 7.69 to 39.56% by the catalyst $HTcMg_2Fe$ and from 4.84% increased to 34.73% by the catalyst $HTcMg_3Fe$. However, at a high catalyst content of 30–60 mg, the percentage removal MDEA solution did not increase therefore the adsorption process, suggesting that it had reached its saturation level as there were no MDEA molecules available to be adsorbed at higher dosages of the catalysts (Nayunigari *et al.* 2017). Thus, the amount of 30 mg for both catalysts used was selected as the optimum amount for subsequent experiments. Additionally, as shown inset in Figure 8(b), the influence of catalyst dosage on both catalysts was studied under the same condition: (solution volume of 100 ml containing 4 Wt% MDEA, flow ozone rate of 5 mg/min, and reaction time of 2 h). Overall, the optimum dosage of both catalysts in the catalytic ozonation process of MDEA depends on the amount of catalyst. Suggesting, in the present study, the value of 30 mg of both catalysts was determined as the optimum dosage for the degradation of MDEA in the catalytic ozonation process. In addition, the ozonation of MDEA with or without a catalyst was performed under the same conditions (pH 10, temperature of 30 °C, and 30 mg catalysts), such as a flow rate O_3 of 5 mg/min with continuous steering. According to results shown in Figure 8(b), it can be seen the efficiency of ozone alone is low and the degradation of pollutants

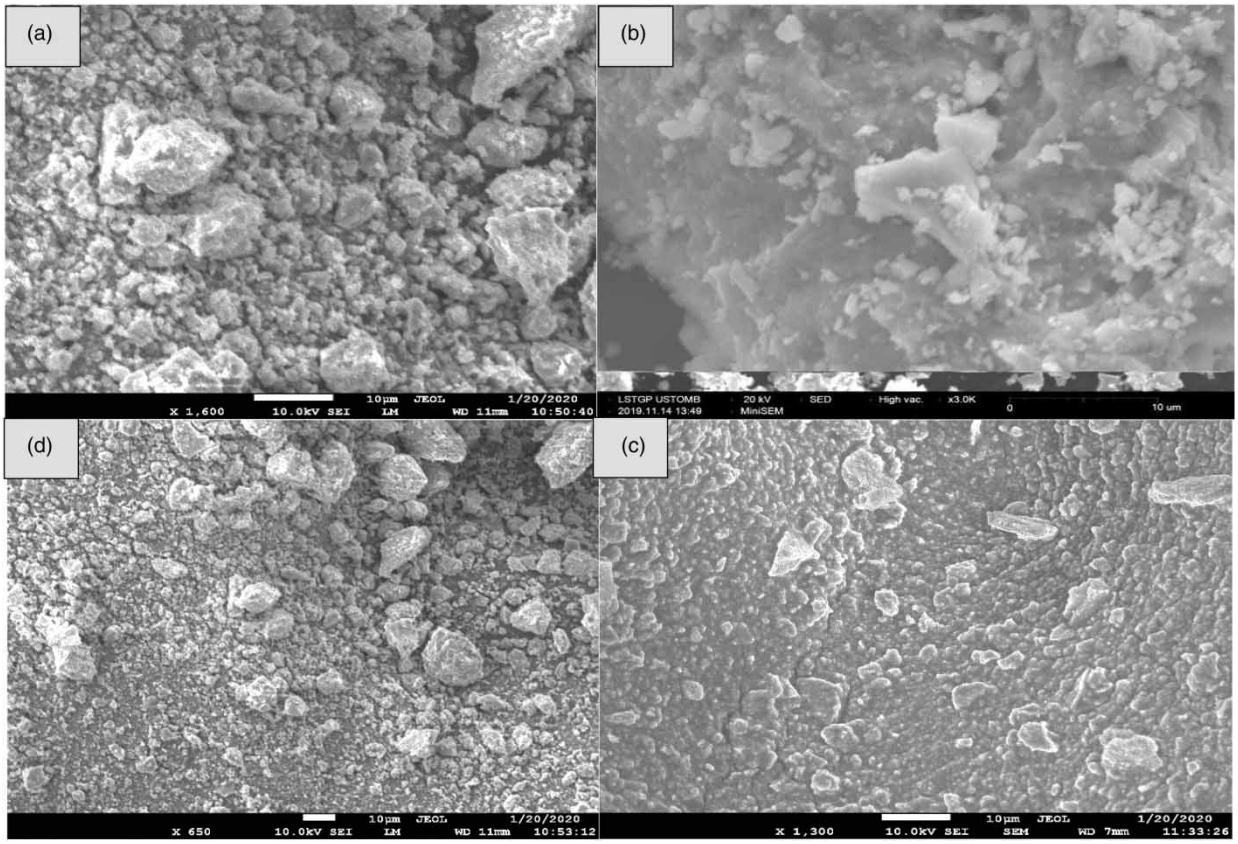

Figure 7 | SEM images of (a) Mg_2Fe-LDH; (b) Mg_3Fe-LDH; (c) $HTcMg_2Fe$; and (d) $HTcMg_2Fe$ materials.

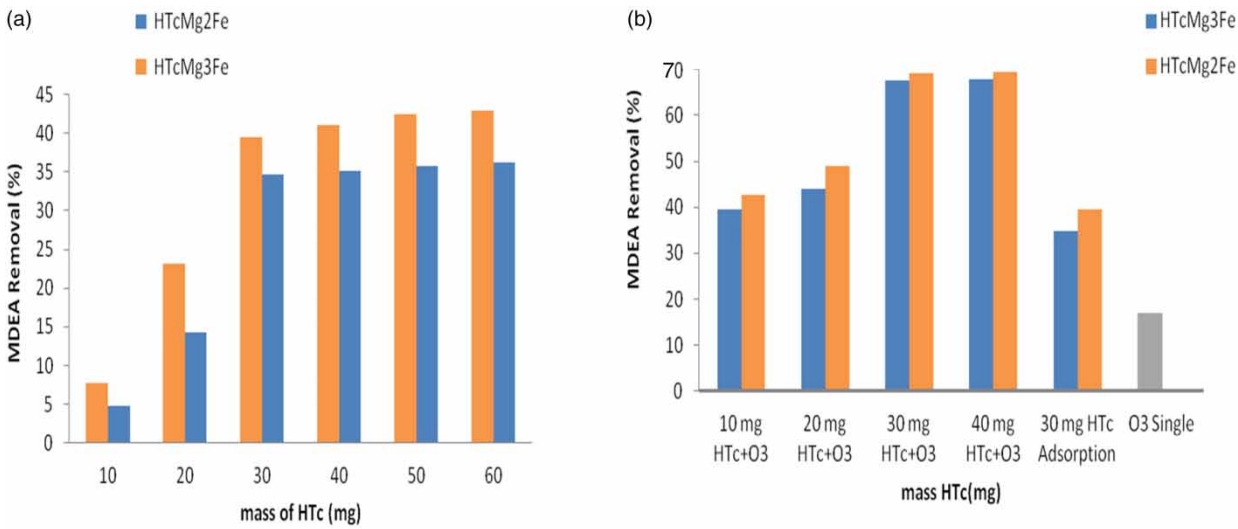

Figure 8 | (a) MDEA removal with different dosages of HTc by adsorption and (b) MDEA removal by adsorption catalytic and no catalytic ozonation with inset: (effect of catalyst mass on catalytic ozonation).

is ineffective, that reduce only 16.92%, which is very slow; due to the low reaction rate of organic compounds with ozone and low solubility and stability of ozone in aqueous solutions and the main disadvantages of the ozonation process. In addition, this procedure has low mineralization efficiency for organic compounds. Therefore, it is essential to modify this process in order to maximize the removal of the pollutants and also intermediate compounds (Esrafil *et al.* 2021). When the catalytic

ozonation process can overcome these problems, during this reaction, the catalysts can promote O_3 decomposition and generate active free radicals $OH^{\cdot}$, which can enhance the degradation of MDEA. As shown in Figure 8(b), the presence of catalysts with an ozone flow rate of 5 mg/min in the process was reduced by 69.23 and 67.69% of MDEA by catalysts $HTcMg_2Fe$ and $HTcMg_3Fe$, respectively. The efficiency of the catalytic process in the presence of the systems (catalysts + O_3) toward reducing MDEA was due to the synergetic effect of both components. The indirect reaction of ozone molecules with organic compounds occurs after ozone degradation and the formation of secondary oxidants, especially radical hydroxyl $OH^{\cdot}$ (Bing *et al.* 2019a, 2019b). The mechanism of ozone reaction with organic compounds in aqueous MDEA solution was according to Equations (4)–(9).

$$O_3 + OH^- \rightarrow O_2 + HO_2^- \quad (4)$$

$$O_3 + HO_2 \rightarrow HO_2^{\bullet} + O_3^{\bullet} \quad (5)$$

$$HO_2 \rightarrow O_2^- + H^+ \quad (6)$$

$$O_3 + O_2^{\bullet -} \rightarrow O_3^{\bullet -} + O_2 \quad (7)$$

$$O_3^{\bullet -} + H^+ \rightarrow HO_3^{\bullet} \quad (8)$$

$$HO_3^{\bullet} \rightarrow O_2 + OH^{\bullet} \quad (9)$$

3.2.2. Effect of the time

The kinetics of ozonation of aqueous MDEA solution in the presence of 30 mg of catalysts was studied at pH 10 and a temperature of 30 °C, the experiments were carried out using a fixed initial concentration of aqueous MDEA solution (4 Wt%), and the ozone gas was introduced through a porous diffuser at the bottom of the reactor at a flow rate of 5 mg/min under continuous steering. A 5 ml of sample was taken every 10 min to separate the catalyst particles by filtration.

As shown in Figure 9, the COD and MDEA percentage removals are plotted as a function of the time. Therefore, the variation in MDEA concentration removal was observed more slowly for the two catalysts in the process (catalysts + O_3) in the first 40 min from the star reaction, after which it continued at a very slow rate of 40–60 min, while the MDEA removal by the process attained 69.23 and 67.69% by the $HTcMg_2Fe$ and $HTcMg_3Fe$, respectively. Eventually, with a sufficient contact time of 60 minutes reaction progress was achieved.

This indicates that the system is in equilibrium, as a result of the saturation of the two catalysts' surface sites. It can be seen from Figure 9(a), the COD removal is achieved after 60 min of reaction catalytic ozonation for both materials, it was observed that the process (catalyst + O_3) was more effective in removing the COD in wastewater containing MDEA, resulting in an average of 80.64 and 80.20% by $HTcMg_2Fe$ and $HTcMg_3Fe$, respectively, in the process (catalyst + O_3). This shows that the prepared ($HTcMg_2Fe$ and $HTcMg_3Fe$) had better catalysts for catalytic ozonation performance. Furthermore, the kinetics of the catalytic ozonation process was also investigated, and it was found that kinetics degradation corresponds to the pseudo-first-order model; which can be described by the following expression:

$$\ln\left(\frac{C_0}{C_t}\right) = kt \quad (10)$$

where C_0 and C_t are MDEA concentration at reaction time t_0 and t, respectively, and k is pseudo-first-order rate constant (min^{-1}). According to the results of the pseudo-first order on both catalysts given in Figure 9(c) and listed in Table 3, it can be seen that the catalytic ozonation with catalysts toward the degradation of MDEA is much higher than in the presence of $HTcMg_2Fe$, while the correlation coefficient ($R^2 = 0.981$), rate constant $k = 0.0201\ min^{-1}$, and $t_{1/2} = 34.48\ min^{-1}$, was higher than for $HTcMg_3Fe$ ($R^2 = 0.973$), rate constant $k = 0.0184\ min^{-1}$, and $t_{1/2} = 37.66\ min^{-1}$.

3.2.3. Effect on initial MDEA concentration

The purpose of the experiments was to investigate the effect of initial MDEA concentrations on the degradation efficiency in (catalysts + O_3) systems, they were performed at a temperature of 30 °C, pH 10, and different MDEA concentrations ranging from 4, 8, 12, 16, and 20 Wt% in a 100 ml aqueous solution containing catalysts mass of 30 mg. Again the solution while magnetic stirring for 60 min. The ozone gas is introduced in a quartz tube with a flow rate of 5 mg/min. 05 ml of samples are taken

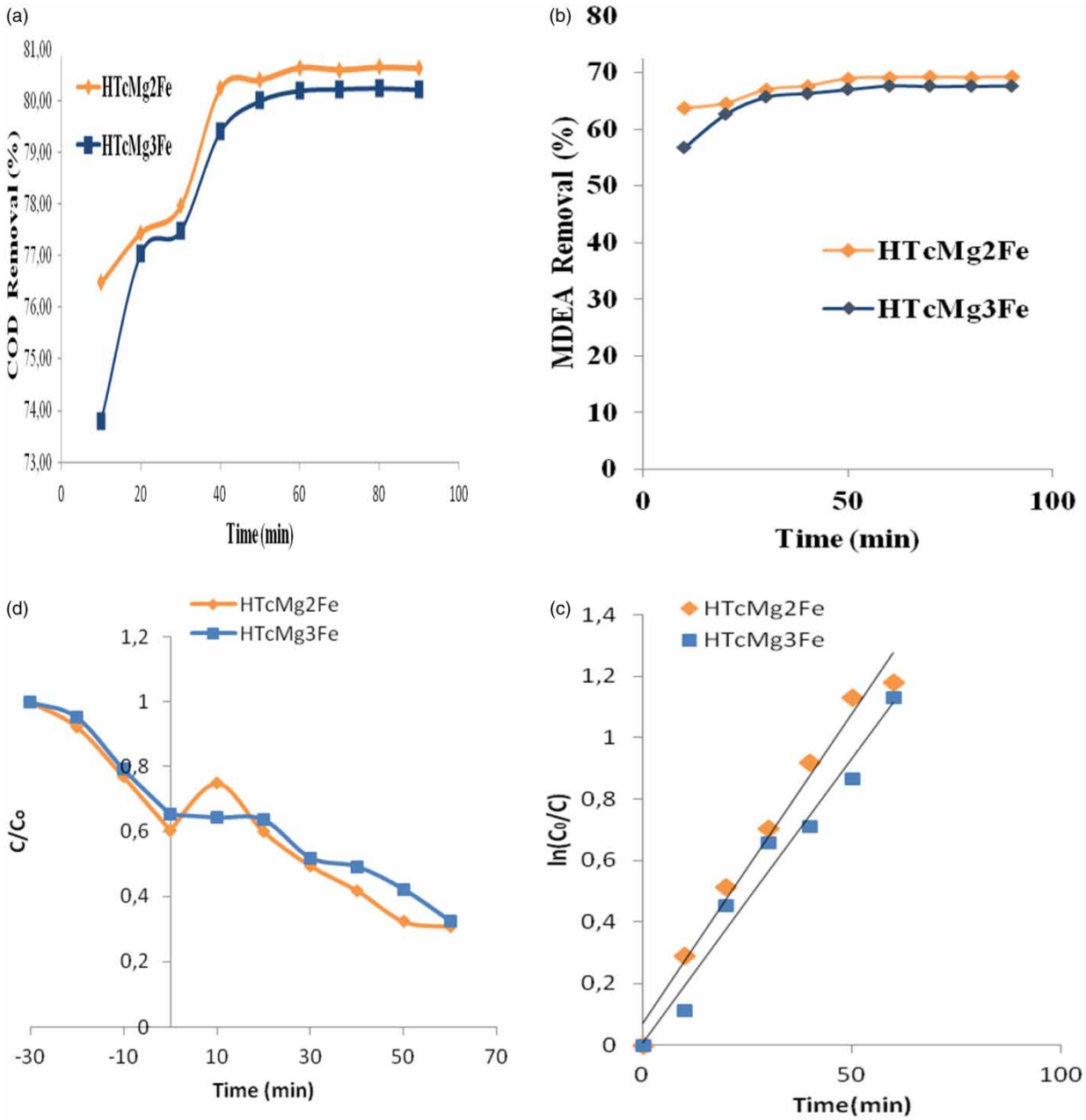

Figure 9 | Effect of time for degradation of MDEA (4 Wt%) by 30 mg HTcs (a) removal percentage of COD, (b) MDEA removal (%), (c) degradation (adsorption, catalytic ozonation), and (d) linear fit of the pseudo-first-order model.

Table 3 | Pseudo-first-order kinetic parameters for degradation of MDEA

Process	Removal (%)	K_{app} (min^{-1})	$t_{1/2}$ (min^{-1})	R^2
$HTcMg_2Fe + O_3$	69.23	0.0201	34.48	0.981
$HTcMg_3Fe + O_3$	67.69	0.0184	37.66	0.973

and filtered through millipore filters (porosity 0.22 μm) in order to remove catalyst particles. Subsequently, the residual MDEA concentrations during the catalytic ozonation were analyzed. As shown, the results obtained during degradation in Figure 10(b).

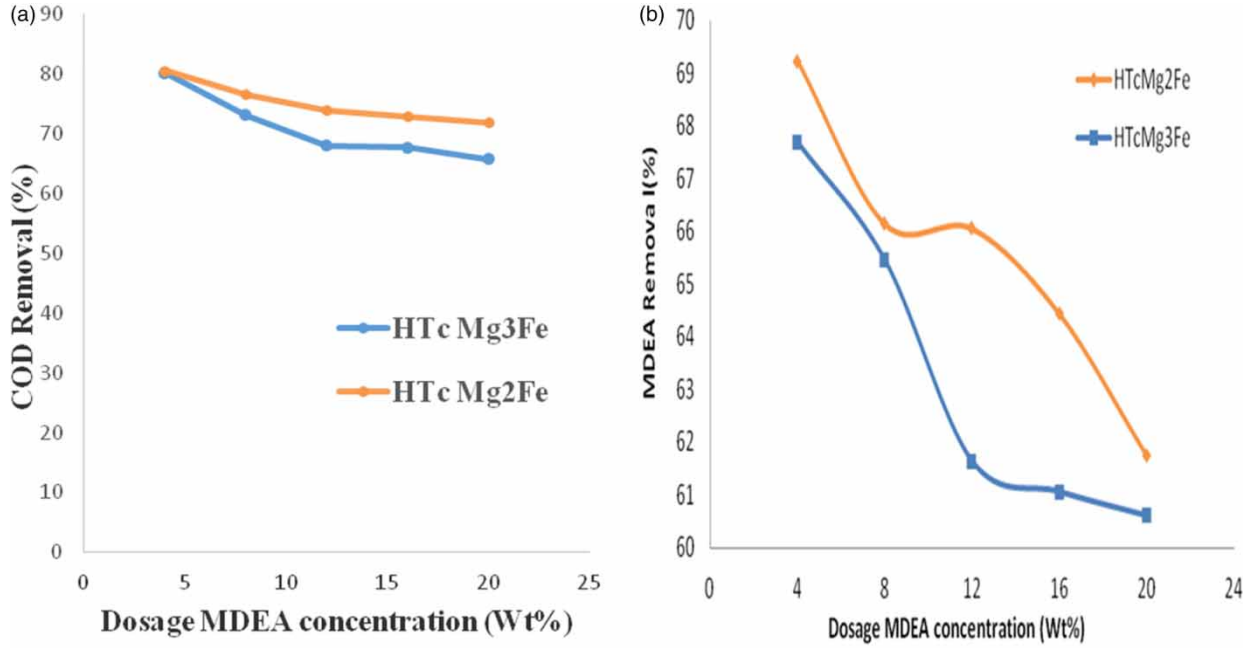

Figure 10 | Effect of initial MDEA concentration on the ozonation catalytic. (a) Reduction percentage of COD and (b) degradation of MDEA (Wt%).

The removal efficiency decreased with the increasing initial concentration of MDEA. This could be attributed to the insufficiency of systems (catalysts + O_3) to remove high MDEA molecules in the aqueous solution. To investigate the performance of this process, the COD analysis was performed under the same conditions (Figure 10(a)). The highest value of the COD removal was (80.64%) obtained when using (4 Wt%) of MDEA, then the COD removal decreased with increasing of MDEA content in the aqueous solution. Overall, these results indicate that both catalysts with ozone could cause a low degree of degradation and mineralization of the highly concentrated MDEA (Gholamreza *et al.* 2009).

3.2.4. Effect of initial pH

The initial pH of the solution is also one of the important parameters in the process of treating the MDEA from aqueous solutions. All experiments were performed with 100 ml of a solution containing (4 Wt%) of MDEA, using the same operating conditions (the temperature of 30 °C, the mass of catalyst 30 mg, and the ozone flow rate of 5 mg/min) in several initial pH values in the range (3–11) by adjusting solutions with 0.01 N NaOH or HCl. As shown in Figure 11, the efficiency of catalytic ozonation treatment of wastewater in different regions, and the efficiency of MDEA was observed at all pH values. The destructive performance slowly increased from low to initially neutral pH levels, but it began to decrease when the basic pH was performed.

The results showed that the highest COD removals were observed over catalysts $HTcMg_2Fe$ up to 80.76% at pH 7 and $HTcMg_3Fe$ at 80.36% at pH 8, due to the reactivity and stability of catalysts in this pH range. In addition, the high removal of MDEA in alkaline pH can be related to pH_{pzc} of catalysts (Andrei *et al.* 2021). The pH_{pzc} of HTc was determined by the solid addition method to be 7.7 for $HtcMg_2Fe$ and 8.2 for $HtcMg_2Fe$. Therefore, the pH_{pzc} is the pH at which the catalyst's surface is electrically neutral can be explained the best removal efficiency was obtained while the high stability of the catalyst. Many studies have reported that in alkaline conditions the performance catalytic ozonation efficiency increases, because the decomposition of ozone generating free active radicals especially $OH^{\cdot}$ radicals), which are extremely oxidizing species and selectively react with organic compounds in aqueous solutions. Additionally, in our study, the destruction performance of MDEA was started in an acidic pH 3 environment and was 77.6% for the process ($HTcMg_2Fe + O_3$) and 77.8% for the process ($HTcMg_3Fe + O_3$). Also in an alkaline solution, the MDEA removal efficiency in the catalytic ozonation reaction was 80.61% in the process ($HTcMg_2Fe + O_3$) and 80.28% in the process ($HTcMg_3Fe + O_3$) at pH 11, under these conditions, it becomes ozone combined with the catalyst increasing the production of hydroxyl radicals $OH^{\cdot}$ can be very reactivity with MDEA solution in the presence of a catalyst, which increases the treatment efficiency of MDEA-wastewater.

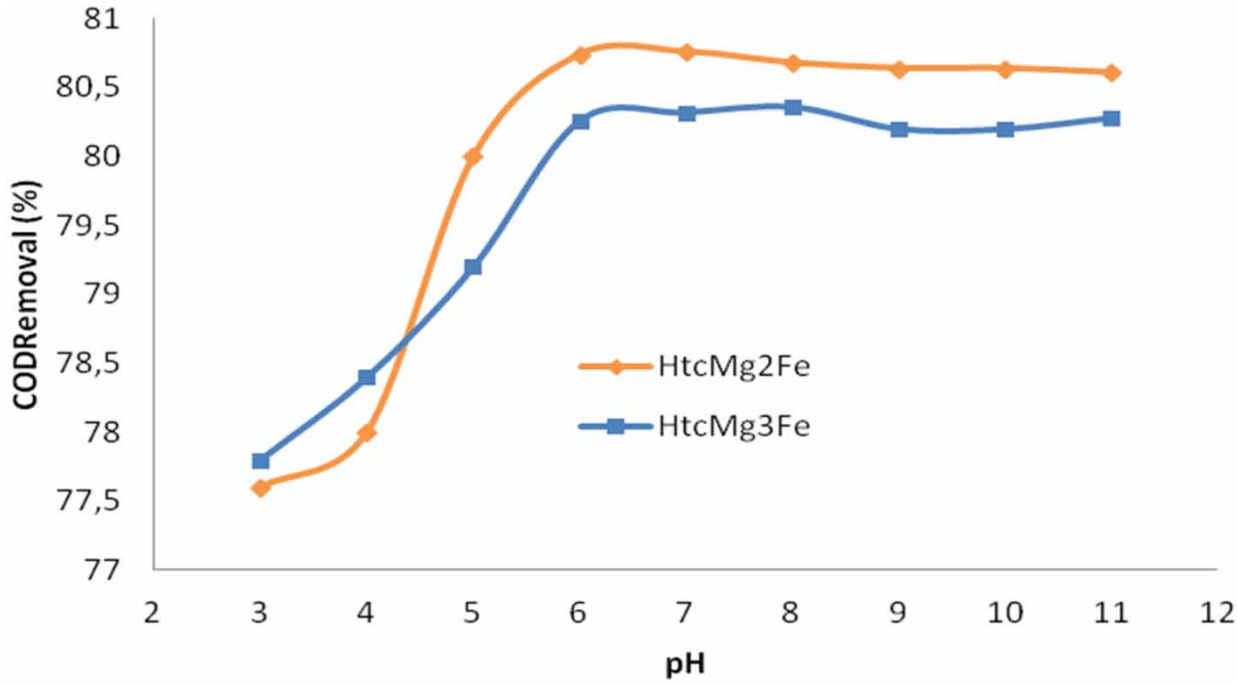

Figure 11 | Effect of pH on the catalytic ozonation of MDEA (4 Wt%). Reduction percentage of COD.

Table 4 | Comparison of this work for degradation MDEA with reported different

References	Process	Concentration MDEA	Flow rate O_3	Removal efficiency
Samira *et al.* (2016)	(UV/$K_2S_2O_8$) process	500 ppm	/	75% COD
Bing *et al.* (2019b)	Fe–C microelectrolysis	MDEA (Puguang Plant in Sichuan Province, China). Mass ratio of filings to wastewater = 1:1	/	96% COD
Mohammad *et al.* (2022)	Subcritical and supercritical water oxidant	1,095 ppm	/	97.4% MDEA dégradation
Gi-Taek *et al.* (2022)	Fenton method O_3 oxidation test	(44–32 mg/L) (44–32 mg/L)	/ 56 mg/L	47.0% COD 27.2% COD
In this study	**($HTcMg_2Fe + O_3$)** **($HTcMg_3Fe + O_3$)**	**4 Wt%** **4 Wt%**	**5 mg/min** **5 mg/min**	**80.76% COD** **80.36% COD**

Both calcined LDH (HTc) have almost the same catalytic activity toward the degradation of MDEA with a mean removal COD of 80.76% in the pH 7 by $HTcMg_2Fe$, this value remained significant when compared to the work of Samira Molareza *et al.*, who used ultraviolet UV light and peroxy disulfate for the photochemical oxidation of MDEA (Samira *et al.* 2016).

The present study for catalytic ozonation of MDEA has been compared with previous research work to understand the novelty of this work (Table 4). From this table, all applied materials ($HtcMg_2Fe$ and $HtcMg_3Fe$) were better catalysts for the removal efficiency of MDEA. Moreover, this study was evaluating the efficiency of catalytic ozonation reaction, which increased the removal of aqueous methyl diethanolamine. Indicating possibilities of applications in industrial as a pre-treatment before a biological process using the system (catalysts + O_3).

4. CONCLUSION

In summary, Mg_2Fe-LDH and Mg_3Fe-LDH are successfully synthesized via the co-precipitation method. A portion of the LDH was calcined at 400 °C for 6 h to obtain two calcined powders designated respectively as $HTcMg_2Fe$ and $HTcMg_3Fe$.

The LDHs powder exhibited rhombohedral symmetry and after activation by calcination, the structure of both LDHs completely collapse to give a mixture of oxides ($MgO + MgFe_2O_4$) with a spinel structure. The study of the catalytic ozonation process for MDEA degradation revealed higher MDEA removal efficiency compared to the direct ozonation process. Overall, both catalysts with ratio R = 2.3 Mg/Fe exhibited the best degradation performance. After 60 min reaction, 30 mg catalysts, (4 Wt%) MDEA, an average value of COD removal was 80.76% obtained by $HTcMg_2Fe$ pH 7 and 80.36% by $HTcMg_3Fe$ at pH 8. Both catalysts showed almost higher COD removal versus MDEA degradation in aqueous solutions with a small improvement for $HTcMg_2Fe$ compared to $HTcMg_3Fe$. Ultimately, after calcination the Mg_2Fe-LDH structure can yield a mixed oxide ($HTcMg_2Fe$), which can be considered as an excellent practical alternative catalyst with high performance in the removal of organic pollutants such as MDEA from aqueous solutions.

ACKNOWLEDGEMENTS

We thank the Algerian University for financial support, for providing various facilities, and for necessary approval.

DATA AVAILABILITY STATEMENT

All relevant data are included in the paper or its Supplementary Information.

CONFLICT OF INTEREST

The authors declare there is no conflict.

REFERENCES

Aaron, L. & Dahn, J. R. 2019 The formation of layered double hydroxide phases in the coprecipitation syntheses of $[Ni_{0.80}Co_{0.15}]_{(1-x)/0.95}Al_x(OH)_2$ $(anion^{n-})x/n(x= 0 - 0.2, n =1,2)$. *Chemical Engineering* **3**, 1–14.

Ali, B., Naceur, B., Abdelkader, E., Karima, E. & Nourredine, B. 2020a Competitive adsorption of binary dye from aqueous solutions using calcined layered double hydroxides. *International Journal of Environmental Analytical Chemistry* **1021**, 3207–3226.

Ali, B., Naceur, B., Abdelkader, E., Karima, E. & Nourredine, B. 2020b Competitive adsorption removal of indigo carmine and Congo red dyes from residual effluents by Zn_2Al-LDH prepared by co-precipitation. *Desalination and Water Treatment* **201**, 404–419.

Amy-Louise, J., Edward, L., Orla, W. & Rachel, L. G. 2021 Understanding layered double hydroxide properties as sorbent materials for removing organic pollutants from environmental waters. *Journal of Environmental Chemical Engineering* **9**, 105197.

Anamália, F. d. S., José, L. d. S. & Duarteab, L. M. 2021 Different routes for MgFe/LDH synthesis and application to remove pollutants of emerging concern. *Separation and Purification Technology* **264**, 118353.

Andrei, I., Marina, R., Taty, K. & Vladimir, P.-I. 2021 A comparative study on the synthesis of magnesium ferrite for the adsorption of metal ions: insights into the essential role of crystallite size and surface hydroxyl groups. *Chemical Engineering Journal* **411**, 128523.

Bert, F. S., Dirk, E. D. V. D. & Pierre, A. J. 2001 Hydrotalcite like anionic clays in catalytic organic reactions. *Catalysis Reviews Science and Engineering* **43**, 443–488.

Bing, W., Huan, Z., Feifei, W., Xingaoyuan, X., Kun, T., Yubo, S. & Tingting, Y. 2019a Application of heterogeneous catalytic ozonation for refractory organics in wastewater. *Catalysts* **9** (3), 241.

Bing, W., Kun, T., Xingaoyuan, X. & Hongyang, R. 2019b Treatment of overhaul wastewater containing *N*-methyldiethanolamine (MDEA) through modified Fe–C microelectrolysis-configured ozonation: investigation on process optimization and degradation mechanisms. *Journal of Hazardous Materials* **369**, 655–664.

Che, N. H., Che, M. & Azizul, B. 2014 Monoethanolamine (MEA) wastewater treatment using photo-Fenton oxidation. *Applied Mechanics and Materials* **625**, 792–795.

Dhal, J.-P., Sethi, M., Mishra, B. G. & Hota, G. 2015 MgO nanomaterials with different morphologies and their sorption capacity for removal of toxic dyes. *Materials Letters* **141**, 267–271.

Esrafil, A., Amir, S.-m., Heshmatollah, N., Shahram, N. & Mohammad, A. 2021 Degradation of ciprofloxacin by photocatalytic ozonation process under irradiation with UVA: comparative study, performance and mechanism. *Process Safety and Environmental Protection* **147**, 356–366.

Esthela, R.-R., Tzompantzi, F.-J., Arturo, B., Norma, L.-G.-O., Clara, T.-F. & Maria, P.-G. H. 2019 Photocatalytic degradation of 2,4,6-trichlorophenol by MgO–MgFe O derived from layered double hydroxide structures. *Catalysts* **63**, 546–563.

Fei-peng, J., Li, S., Jin-gang, Y., Xin-yu, J., Xiao-qing, C. & Shao-long, D. 2014 Adsorption of glutamic acid from aqueous solution with calcined layered double Mg–Fe–CO_3 hydroxide. *Transactions of Nonferrous Metals Society of China* **24**, 3971–3978.

Gholamreza, M., Ali, K. & Rahimeh, A. 2009 The investigation of catalytic ozonation and integrated catalytic ozonation/biological processes for the removal of phenol from saline wastewaters. *Journal of Hazardous Materials* **171**, 175–181.

Gi-Taek, O., Chi-Kyu, A. & Min-Woo, L. 2022 Advanced oxidation pretreatment for biological treatment of reclaimer wastewater containing high concentration *N*-methyldiethanolamine. *Applied Science* **12** (8), 3960.

Haithem, B. H., Maria, E. G., Mourad, B. Z. & Patrick, D. C. 2019 TiO_2/Clay as a heterogeneous catalyst in photocatalytic/photochemical oxidation of anionic reactive blue 19. *Arabian Journal of Chemistry* **12**, 1454–1462.

Haolan, L., Yuanyuan, J., Ruru, Z., Zhili, C. & Zhaoyin, H. 2022 Co-production of hydrogen and acetaldehyde from ethanol over a highly dispersed Cu catalyst. *Fuel* **321**, 123980.

Haung, S. K., Yoo, S. P., Chiho, K., Yeong, K., Jooyoung, L., Hyunsoo, J., Yoon, S. L., Sung, M. C. & Yangdo, K. 2020 Self-assembly of Ni–Fe layered double hydroxide at room temperature for oxygen evolution reaction. *Energy Reports* **6**, 248–254.

Hrvoje, K., Natalija, K. & Ana, L. B. 2006 Minimization of organic pollutant content in aqueous solution by means of AOPs: UV-and ozone-based technologies. *Chemical Engineering Journal* **123**, 127–137.

Hui, L., Feng, Z., Jing, W., Jianmin, Z., Xiaohui, H., Lai, C., Pengfei, H., Jian-ming, G., Qiang, Z., Sajid, B. & Jingbo, L.-L. 2020 Facile preparation of zeolite-activated carbon composite from coal gangue with enhanced adsorption performance. *Chemical Engineering Journal* **390**, 124513.

Jiapeng, Y., Hui, W., Rong, H. & Yijun, C. 2022 The heterogeneous Fenton degradation of persistent organic pollutants using natural chalcopyrite: effect of water matrix and catalytic mechanism. *Environmental Science and Pollution Research* **29**, 75651–75663.

Laila, J., Bander, J. & Raphael, I. 2018 Screening study for selecting new activators for activating MDEA for natural gas sweetening. *Separation and Purification Technology* **199**, 320–330.

Legube, B. & Karpel, N. V.-L. 1999 Catalytic ozonation: a promising advanced oxidation technology for water treatment. *Catalysis Today* **53**, 61–72.

Ligita, V., Marina, R., Inga, G.-P., Vladimir, P., Aleksej, Z., Andrei, I. & Aivaras, K. 2020 On the reconstruction peculiarities of sol–gel derived $Mg_{2-x}M_x/Al_1$ (M = Ca, Sr, Ba) layered double hydroxides. *Crystals* **10** (6), 470.

Lim, S., Shi, J. L., von Gunten, U. & McCurry, D. L. 2020 Minimization of organic pollutants content in aqueous solution by means of AOPs: UV- and ozone-based technologies. *Water Research* **213**, 118053.

Lingyu, Z., Jingxin, L., Aimin, L., Jianing, S., Jiangyan, X. & Hongmei, J. 2022 Controllable synthesis of cubic magnetic $MgFe_2O_4$ derived from MgFe-LDHs for efficient removal of methyl orange. *Chemical Engineering Journal* **428**, 131174.

Mahesh, M. M., Hoang, Y. & Freddy, K. 2014 Nanocatalyst mesoporous mixed metal oxides for catalytic applications [Nanomoulage d'oxydes mixtes mésoporeux pour des applications catalytiques]. *Comptes Rendus Chimstry* **17**, 641–655.

Masoud, S., Afshin, T. M., Seyed, A. H. & Sakineh, M. 2021 Mg-Al LDH and calcined LDH: green nanocatalysts for wet peroxide oxidation of phenol in wastewater. *Journal of Water and Environmental Nanotechnology* **6**, 72–80.

Mir Saeed, E., Zahra, V., Reza, T.-L. & Ali, M. 2021 Preparation and study of the catalytic application in the synthesis of xanthenedione pharmaceuticals of a hybrid nano-system based on copper, zinc and iron nanoparticles. *Research on Chemical Intermediates* **47**, 973–996.

Mohammad, M., Yousef, D. S., Karthik, K. & Hakimeh, M. 2020 Degradation of p-nitroaniline from aqueous solutions using ozonation/Mg-Al layered double hydroxides integrated with these quencing batch moving bed biofilm reactor. *Journal of the Taiwan Institute of Chemical Engineers* **113**, 241–252.

Mohammad, N.-G., Feridun, E., Dariush, M. & Abbas, E. 2022 Treatment of methyldiethanolamine wastewater using subcritical and supercritical water oxidation: parameters study, process optimization and degradation mechanism. *Environmental Science and Pollution Research* **29** (655), 1–15.

Nayunigari, M. K., Das, R. & Maity, A. 2017 Folic acid modified cross-linked cationic polymer, synthesis characterization and application of the removal of Congo red due from aqueous medium. *Journal of Molecular Liquids* **227**, 87–97.

Nazrizawati, A. T., Jinesh, C. M., Adam, F. L. & Karen, W. 2022 Alkali-free hydrothermally reconstructed NiAl layered double hydroxides for catalytic transesterification. *Catalysts* **12** (3), 286.

Oller, I., Malato, S. & Sánchez-Pérez, J. A. 2011 Combination of advanced oxidation processes and biological treatments for wastewater decontamination – a review. *Science of The Total Environment* **409** (20), 4141–4166.

Qining, W., Quanwang, Y., Yu, Z., Jie, R. & Ning, A. 2022 Preparation of amine-modified Cu-Mg-AlLDH composite photocatalyst. *Nanomaterials* **12**, 1–17.

Razali, M., Yunus, R., Jemaat, Z. & Alias, S. 2010 Monoethanolamine wastewater treatment via adsorption method; a study on comparison of chitosan, activated carbon, alum and zeolite. *Journal of Applied Sciences* **10** (21), 2544–2550.

Samira, G.-M., Mojtaba, A. & Zinati, Z. 2016 Photochemical oxidation of methyldiethanolamine (MDEA) in aqueous solution by UV/$K_2S_2O_8$ process. *International Journal of Industrial Chemistry* **7**, 1–8.

Shanza, R. K., Saba, J., Shahid, A., Safyan, A. K., Muhammad, M. & Muhammad, R. S. A. J. 2020 Synthesis and structure of calcium-tin hybrid microparticles from eggshell and investigation of their thermal behavior and catalytic application. *Journal of Chemical Physics* **530**, 110613.

Shutang, L., Haomiao, X., Longlong, W., Leipeng, J., Xianwei, L., Zan, Q. & Naiqiang, Y. 2021 Dual-functional sites for selective adsorption of mercury and arsenic ions in $[SnS_4]^{4-}$/MgFe-LDH from wastewater. *Journal of Hazardous Materials* **403**, 123940.

Vaccari, A. 1999 Clays and catalysis: a promising future. *Applied Clay Science* **14**, 161–198.

Violante, A., Cozzolino, V., Perelomov, L., Caporale, A. G. & Pigna, M. 2010 Mobility and bioavailability of heavy metals and metalloids in soil environments. *Journal of Soil Science and Plant Nutrition* **10** (3), 268–292.

Xiangbo, S., Yuhe, L., Yuting, P. S., Lungang, C., Longlong, M., Hongwei, Y. & Chenguang, W. 2021 Highly effective production of 5-hydroxymethyl furfural from fructose with a slow-release effect of proton of a heterogeneous catalyst. *Energy and Fuels* **35**, 16665–16676.

Yi, L., Pingan, Y., Yanhong, L., Dandan, W., Jiasai, L., Shuhui, W., Fang, W., Liang, F. & Yu, P. 2021 Facile synthesis of NiFe-layered double hydroxide and mixed metal oxide with excellent microwave absorption properties. *Molecules* **26**, 5046.

Yuanfeng, Q. C. G., Xing, X., Baoyu, G., Qinyan, Y., Bo, J., Zhou, Q., Changzhi, W. & Yanqing, Z. 2020 Co/Fe and Co/Al layered double oxides ozone catalyst for the deep degradation of aniline: preparation, characterization and kinetic model. *Science of The Total Environment* **715**, 136982.

Yuanxing, H., Tingting, Y., Manli, L., Yaowei, W., Zhihua, X., Daofang, Z. & Liang, L. 2019 Ni-Fe layered double hydroxides catalyzed ozonation of synthetic wastewater containing Bisphenol A and municipal secondary effluent. *Chemosphere* **235**, 143–152.

Zhenxing, Z., Tianbao, L., Jinxiong, W., Hongling, L., Shasha, C., Xiaoquan, Z., Lijuan, Z., Jing, L., Andrei, I., Bekchanov, D., Kongjun, M. & Xintai, S. 2023 Preparation of copper-based catalysts from electroplating sludge by ultrasound treatment and their antibiotic degradation performance. *Environmental Research* **216**, Part 2114567.

First received 16 July 2022; accepted in revised form 24 March 2023. Available online 6 April 2023